(2+1) Resonance-enhanced ionization spectroscopy of a state-selected beam of OH radicals

Margaret E. Greenslade and Marsha I. Lester[a)]
Department of Chemistry, University of Pennsylvania, Philadelphia, Pennsylvania 19104-6323

Dragana Č. Radenović, André J. A. van Roij, and David H. Parker
Department of Molecular and Laser Physics, University of Nijmegen, Toernooiveld 1, 6525 ED, Nijmegen, The Netherlands

(Received 11 March 2005; accepted 17 June 2005; published online 22 August 2005)

A state-selected beam of hydroxyl radicals is generated using a pulsed discharge source and hexapole field. The OH radicals are characterized by resonance-enhanced multiphoton ionization (REMPI) spectroscopy via the nested $D\,^2\Sigma^-$ and $3\,^2\Sigma^-$ Rydberg states. Simplified spectra are observed from the selected $|M_J|=3/2$ component of the upper Λ-doublet level of the lowest rotational state ($J=3/2$) in ground ($v''=0$) and excited ($v''=1-3$) vibrational levels of the OH $X\,^2\Pi_{3/2}$ state. Two-photon transitions are observed to the $D\,^2\Sigma^-(v'=0-3)$ and $3\,^2\Sigma^-(v'=0,1)$ vibronic levels, extending previous studies to higher vibrational levels of the Rydberg states. Spectroscopic constants are derived for the Rydberg states and compared with prior experimental studies. Complementary first-principle theoretical studies of the properties of the $D\,^2\Sigma^-$ and $3\,^2\Sigma^-$ Rydberg states [see M. P. J. van der Loo and G. C. Groenenboom, J. Chem. Phys. **123**, 074310 (2005), following paper] are used to interpret the experimental findings and examine the utility of the (2+1) REMPI scheme for sensitive detection of OH radicals. © *2005 American Institute of Physics*. [DOI: 10.1063/1.1997132]

I. INTRODUCTION

The atmosphere, combustion, and interstellar space are some of the environments where the hydroxyl radical (OH) plays an important role. Typically, laboratory and field measurements of OH radicals are achieved through laser-induced fluorescence (LIF) detection on various well-characterized $A\,^2\Sigma^+$-$X\,^2\Pi$ transitions.[1–5] The utility of the A-X band system is limited to the detection of low vibrational levels of the $X\,^2\Pi$ state, namely, $v''\leqslant 4$,[6] due to Frank-Condon factors that favor diagonal transitions and electronic predissociation in the $A\,^2\Sigma^+$ state. More recently, the $B\,^2\Sigma^+$-$X\,^2\Pi$ system has been developed for LIF detection of higher vibrational levels of the $X\,^2\Pi$ state ($6\leqslant v''\leqslant 15$).[7–11] Nevertheless, certain applications, such as crossed molecular-beam scattering[12,13] and ultracold molecule studies,[14,15] would benefit from even more sensitive detection of OH radicals, such as might be provided by a resonance-enhanced ionization scheme.

Several resonance-enhanced ionization schemes have been developed for OH radicals,[16–19] but these have not been widely adopted for OH detection. Most of the studies utilize the lowest-lying Rydberg states of OH, the nested $D\,^2\Sigma^-$ and $3\,^2\Sigma^-$ states at 10.1 and 10.9 eV, as resonant intermediate states, as illustrated in Fig. 1. The properties of these Rydberg states have been studied by direct absorption,[20] (2+1) resonance-enhanced multiphoton ionization (REMPI) spectroscopy,[17,18] and (1+1) REMPI,[16] the latter resolving a long-standing discrepancy in the location of the $D\,^2\Sigma^-(v'=0)$-$X\,^2\Pi(v''=0)$ band origin. These experimental studies used a variety of ways to produce the OH radicals, namely, photolysis of hydrogen peroxide or formic acid[16–18] and a discharge source.[20] Overall, these studies have enabled characterization of several low vibrational levels of the $D\,^2\Sigma^-(v'=0-2)$ and $3\,^2\Sigma^-(v'=0)$ Rydberg states of the OH radical. The present work builds on the earlier studies by using a jet-cooled and state-selected beam of OH radicals for photoionization studies, and comparing the experimental results with first-principle calculations of the excitation and decay processes that are detailed in the accompanying paper.[21] For example, these calculations show that the initial two-photon $D\,^2\Sigma^- \leftarrow\leftarrow X\,^2\Pi$ excitation step has a reasonably strong absorption cross section. This suggests that (2+1) REMPI detection of OH could be quite effective, if the $D\,^2\Sigma^-$ and $3\,^2\Sigma^-$ states can be ionized efficiently compared to other decay processes.

The current experimental study along with previous studies have been guided by *ab initio* calculations performed more than twenty years ago by van Dishoeck and co-workers.[22,23] These theoretical studies employed configuration-interaction methods to characterize the low-lying electronic states of the OH radical with $^2\Sigma^+$, $^2\Sigma^-$, $^2\Pi$, and $^2\Delta$ symmetries, many of which are involved in photodissociation processes. The potential-energy curves and strongly R-dependent transition dipole moments connecting the states were the main focus of these studies, which also included calculation of photodissociation spectra for transitions from $X\,^2\Pi(v'')$ to repulsive potentials and bound states that subsequently dissociate. Most relevant to the present study were calculations of electronic transition moments and/or oscilla-

a)Author to whom correspondence should be addressed. Fax: (215) 573-2112. Electronic mail: milester@sas.upenn.edu

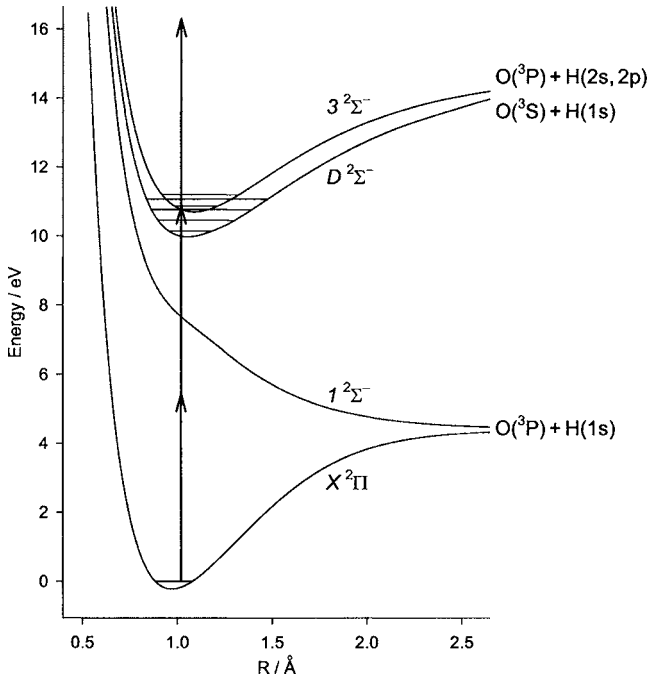

FIG. 1. *Ab initio* potentials computed for the ground $X\,^2\Pi$, repulsive $1\,^2\Sigma^-$, and $D\,^2\Sigma^-$ and $3\,^2\Sigma^-$ Rydberg states of OH from Ref. 21. The (2+1) REMPI transition from the ground state to the $v'=0$ level of the $3\,^2\Sigma^-$ Rydberg state is illustrated.

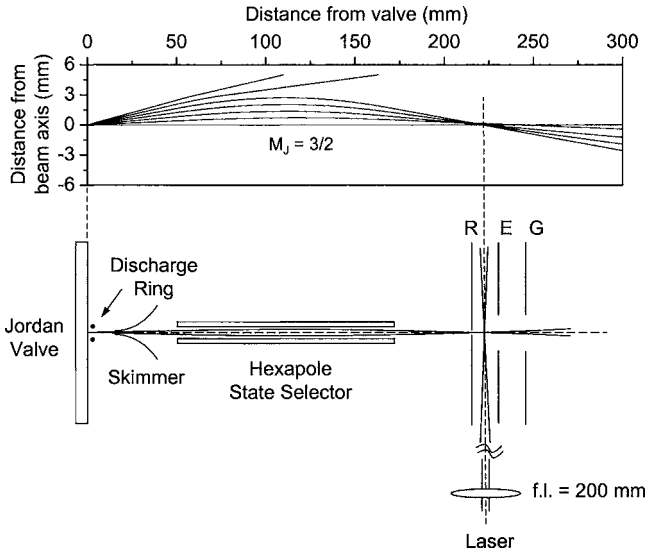

FIG. 2. The experimental apparatus consists of a pulsed discharge source to generate OH radicals, a hexapole field to state select and spatially focus the OH radicals into the laser interaction region, and a time-of-flight (TOF) mass spectrometer with repeller (R), extractor (E), and ground (G) plates shown. The focusing curves (upper panel) show the trajectories for the selected $|M_J|=3/2$ component of the upper Λ-doublet level (f symmetry) of the lowest rotational state of OH ($X\,^2\Pi_{3/2}, J=3/2$). Note that the y-axis scale has been expanded by a factor of six in the upper panel to show the displacement from the beam axis.

tor strengths for one-photon transitions from the $X\,^2\Pi$ to $D\,^2\Sigma^-$ and $3\,^2\Sigma^-$ states as well as the $1\,^2\Sigma^-$ repulsive potential accessed in a recent photodissociation study by this group.[24] The oscillator strength was predicted to falloff smoothly with increasing vibrational excitation in the $D\,^2\Sigma^-$ state,[23] suggesting that higher vibrational levels of the Rydberg states might be observable. The spontaneous emission rate from various $D\,^2\Sigma^-(v')$ states ($\sim 10^8\ s^{-1}$) was also evaluated, although the relative importance of predissociation resulting from crossings with several repulsive potentials ($B\,^2\Sigma^+$, $2\,^2\Pi$, and $1\,^4\Pi$) was not determined in these early calculations.

The following paper[21] presents a comprehensive theoretical investigation of the properties of the $D\,^2\Sigma^-$ and $3\,^2\Sigma^-$ Rydberg states, which are obtained using modern multireference configuration-interaction methods with the MOLPRO package.[25–27] New *ab initio* potentials are computed and then adjusted to ensure that the bound states match the vibrational energies $[G(v)]$ and rotational constants (B_v) observed experimentally. Time-independent perturbation theory is subsequently used to compute one- and two-photon absorption cross sections for transitions from the $X\,^2\Pi$ to $D\,^2\Sigma^-$ and $3\,^2\Sigma^-$ Rydberg states. This involves calculation of the R-dependent transition dipole moments connecting these states as well as the $1\,^2\Sigma^-$ repulsive potential that serves as the dominant virtual state in the two-photon excitation process. In addition, the theoretical study examines the lifetimes of various vibrational levels in the $D\,^2\Sigma^-$ and $3\,^2\Sigma^-$ states resulting from radiative and predissociative decay processes, the latter arising from spin-orbit coupling with the $B\,^2\Sigma^+$, $2\,^2\Pi$, and/or $1\,^4\Pi$ states. The calculated two-photon cross sections and excited-state lifetimes are utilized in the current paper to help interpret the spectroscopic observations from (2+1) REMPI studies of state-selected OH radicals.

The current study also builds on this group's recent investigation of the photodissociation of OD radicals at 226 and 243 nm,[24] which fall within the wavelength region used for REMPI studies. The photodissociation study used velocity map imaging to probe the angle-speed distribution of the D (^2S) and O (^3P) products. Both experiment and complementary first-principle theory showed that photodissociation at these wavelengths results from the promotion of OD from vibrationally excited levels of the ground $X\,^2\Pi$ state to the repulsive $1\,^2\Sigma^-$ potential in a one-photon process. The vibrationally excited OH/D radicals are produced in a discharge source. The present study utilizes this same discharge source, thereby providing an opportunity to investigate REMPI transitions originating from excited vibrational levels of the $X\,^2\Pi$ state for the first time.

II. EXPERIMENT

Several novel experimental techniques are combined in a new vacuum apparatus in Nijmegen to investigate the photodissociation[24] and photoionization of OH radicals. The various components of the experimental apparatus are illustrated in Fig. 2. The OH radicals are produced in a pulsed discharge source[28] that operates as follows: the vapor over liquid H_2O at room temperature is seeded in Ar carrier gas (1.5 bar) and pulsed from a Jordan valve into the primary vacuum chamber. The valve has a conical-shaped stainless-steel nozzle with a 0.4 mm orifice. A stainless-steel ring (4 mm diameter, 0.5 mm thick), which is located on axis 2.5 mm from the orifice, has a high-voltage pulse applied to it that creates an electrical discharge between the ring and the

grounded valve body. The desired OH radicals, as well as other ions and neutral fragments, are produced in the discharge. The production of OH radicals is optimized with a ring voltage of −1.55 kV. The gas pulse is skimmed as it passes into the detection chamber.[29]

A hexapole field is applied in the detection chamber to state select and focus the OH radicals in the gas pulse.[30–33] The hexapole assembly consists of six highly polished cylindrical rods, each of 3 mm diameter and 120 mm length, that are held in a hexagonal array with an internal diameter of 6 mm. The six rods are alternately charged to +7 and −7 kV under typical operating conditions. The hexapole field is used to select the $|M_J|=3/2$ component of the upper Λ-doublet level (f symmetry) of the lowest rotational state of OH ($X\,^2\Pi_{3/2}, J=3/2$). A high degree of state selection is achieved without a beam stop. The hexapole field also acts as an electrostatic lens to spatially focus the state-selected OH radicals on the molecular-beam axis. Calculated trajectories[34] for the state-selected OH beam in the hexapole field are shown in the top panel of Fig. 2. The field defocuses other internal energy states of OH,[30] and has no effect on other species (e.g., O or H_2O) originating from the pulsed discharge source.

A UV laser crosses the state-selected OH radical beam in the ionization region of the time-of-flight (TOF) mass spectrometer that lies along the molecular-beam axis beyond the exit of the hexapole assembly. A frequency-tripled Nd:YAG (yttrium aluminum garnet) laser (Continuum Surelite, 10 Hz, 4–6 ns) pumps a Continuum TDL60 dye laser (0.12 cm^{-1} bandwidth) operating with Coumarin 102, 47, 120, or 307 or Stilbene 420 dye in methanol solution. The ~20 mJ/pulse output from the dye laser in the 430–520 nm region is frequency-doubled with a beta barium borate (BBO) crystal mounted on a tracking stage to yield 2–3 mJ of tunable radiation from 215–260 nm. The UV laser beam is then focused into the ionization region with a 200 mm focal length lens. The laser polarization is vertical and parallel to the TOF detector. The dye laser is calibrated with the well-known (2+1) REMPI spectra of O_2 as well as the (2+1) REMPI lines for NO and O (^3P_J).[35–37] The OH REMPI spectra are more precisely calibrated by simultaneously recording a Ne optogalvanic spectrum using the residual fundamental output of the dye laser.[37,38]

Ions are detected on the OH^+ mass channel ($m/e=17$) using a TOF mass spectrometer that has been specially adapted for velocity map imaging experiments.[39] The electrostatic lens consists of repeller, extractor, and ground plates, each with central holes to allow the molecular beam to pass through them.[40] The extracted ions pass through a field-free region (360 mm) and are then detected using a pair of microchannel plates (MCP) followed by a phosphor screen. The MCP plates are pulsed on to coincide with the arrival time of the desired ion mass. The voltage applied to the second plate is delayed relative to the first plate to discriminate against high-energy photons created directly in the discharge source. A charge-coupled device (CCD) camera mounted behind the phosphor screen captures the images. The data collection is powered by the DaVis software package. The intensity of the ion signal in a rectangular region of the image is accumulated for a fixed number of laser shots before the laser is stepped in wavelength. The process is then repeated until the desired wavelength range is covered in the REMPI spectrum.

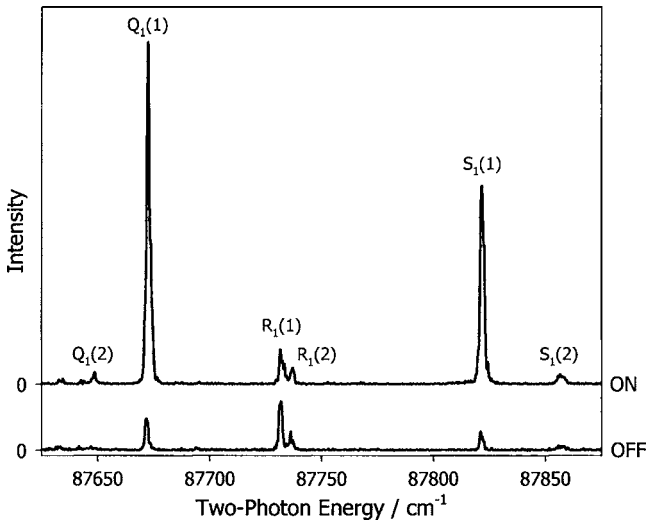

FIG. 3. Comparison of the vibronic band structure observed by (2+1) REMPI for the OH $3\,^2\Sigma^-(v'=0)-X\,^2\Pi(v''=0)$ transition with hexapole focusing on and off. The $Q_1(1)$ and $S_1(1)$ lines that originate from the selected OH ($J=3/2, f$) state are significantly enhanced with hexapole focusing.

III. RESULTS AND ANALYSIS

The jet-cooled molecular beam of OH results in a greatly simplified (2+1) REMPI spectra for OH in the $D\,^2\Sigma^-$-$X\,^2\Pi$ and $3\,^2\Sigma^-$-$X\,^2\Pi$ spectral regions as compared to previously reported spectra.[17,18] A representative spectrum of the two-photon OH $3\,^2\Sigma^-(v'=0)$-$X\,^2\Pi(v''=0)$ transition is shown in Fig. 3 (lower trace, hexapole off). The vibronic band consists of just a few distinct Q_1, R_1, and S_1 lines originating from the lowest rotational levels, $J=3/2$ and 5/2, of the ground $X\,^2\Pi_{3/2}$ state of OH, which illustrates the extensive rotational cooling in the supersonic expansion. Only lines in the Q, R, and S branches are observed due to a combination of two-photon selection rules ($\Delta J=0,\pm1,\pm2$) and Hönl-London considerations at low J.[41]

Further spectral simplification and enhanced sensitivity are achieved through hexapole focusing that selects the $|M_J|=3/2$ component of the upper Λ-doublet level (f symmetry) of the lowest rotational state of OH ($X\,^2\Pi_{3/2}, J=3/2$). This is illustrated in Fig. 3, where the OH $3\,^2\Sigma^-(v'=0)$-$X\,^2\Pi(v''=0)$ transition is shown under hexapole focusing conditions (upper trace, hexapole on), which was recorded immediately after the hexapole off scan. Hexapole focusing results in an eightfold enhancement of the $Q_1(1)$ and $S_1(1)$ lines that originate from the selected OH state ($J=3/2, f$). A slight decrease is observed for the $R_1(1)$ line that originates from the lower Λ doublet of e symmetry, which is defocused by the hexapole field.

Previous LIF measurements with a similar OH discharge source and hexapole field revealed a similar eightfold enhancement for transitions originating from the upper Λ doublet, but a more significant fourfold decrease in intensity for transitions that originate from the lower Λ doublet.[42] In the

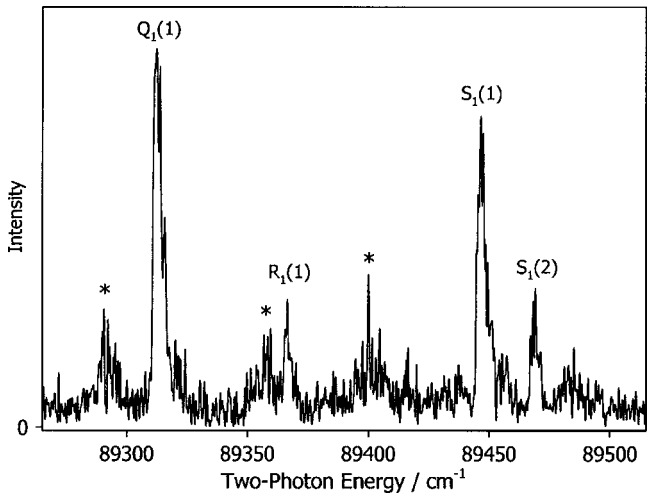

FIG. 4. Vibronic spectrum of the newly observed OH $D\,^2\Sigma^-(v'=3)-X\,^2\Pi(v''=0)$ transition obtained by (2+1) REMPI with hexapole focusing. Asterisks indicate peaks likely due to unassigned (2+1) REMPI transitions of H_2O.

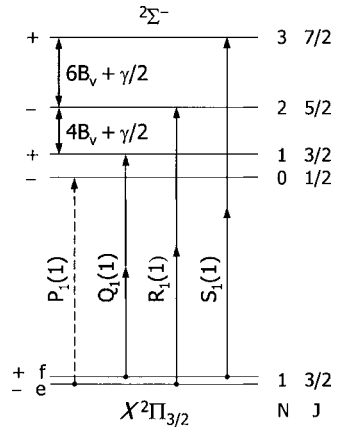

FIG. 6. Energy level diagram illustrating the upper and lower states involved in two-photon $^2\Sigma^-$-$^2\Pi$ transitions. The $Q_1(1)$ and $S_1(1)$ lines are enhanced by hexapole focusing of the upper Λ-doublet level (f symmetry) of the lowest rotational state of OH $X\,^2\Pi_{3/2}(J=3/2)$. The Λ-doublet spacing is exaggerated for clarity. Upper state spacings used to determine the rotational constants via combination differences are noted. The vibronic origin T_v is equivalent to the unobserved $P_1(1)$ transition frequency.

present experiment, the $Q_1(1)$ and $S_1(1)$ line intensities grow as expected, but the $R_1(1)$ line does not decrease as much as expected. This arises from the high voltage applied to the electrostatic lens of the TOF mass spectrometer, which creates an electric field that mixes Λ-doublet states with the same total angular momentum (e.g., $J=3/2$) after hexapole state selection.[43,44] When the high voltage on the electrostatic lens is turned off, the $R_1(1)$ line intensity decreases to the point that it is not observable with the hexapole on.

The enhanced sensitivity for (2+1) REMPI spectra of OH with hexapole focusing of the jet-cooled molecular beam has enabled us to observe several new vibronic bands that have not been reported previously. Transitions have been identified to higher vibrational levels of the $D\,^2\Sigma^-$ and $3\,^2\Sigma^-$ Rydberg states than seen previously, as shown in Figs. 4 and 5. The rotational band structure associated with the $D\,^2\Sigma^-(v'=3)$-$X\,^2\Pi(v''=0)$ and $3\,^2\Sigma^-(v'=1)$-$X\,^2\Pi(v''=0)$ transitions are displayed in the figures. These bands are assigned based on their vibrational spacing from the next lower

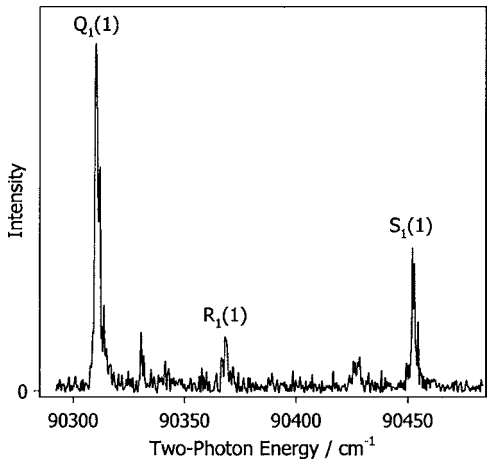

FIG. 5. Rotational band structure associated with the newly observed OH $3\,^2\Sigma^-(v'=1)-X\,^2\Pi(v''=0)$ transition obtained by (2+1) REMPI with hexapole focusing.

level, the characteristic three line rotational band structure, $Q_1(1)$, $R_1(1)$, and $S_1(1)$, under jet-cooled conditions, and the enhancement of the $Q_1(1)$ and $S_1(1)$ lines with hexapole focusing (only hexapole on conditions are shown in the figures). The OH $D\,^2\Sigma^-(v'=3)$-$X\,^2\Pi(v''=0)$ spectral region (Fig. 4) is complicated by the appearance of three weak features near 89 290, 89 360, and 89 400 cm^{-1}, which are likely due to unassigned (2+1) REMPI transitions of H_2O.[45] In addition, transitions are observed for all lower vibrational levels of these Rydberg states, $D\,^2\Sigma^-(v'=0-2)$ and $3\,^2\Sigma^-(v'=0)$, from the hexapole state-selected OH $X\,^2\Pi_{3/2}(v''=0,J=3/2,f)$ level. Searches were made for transitions that access yet higher vibrational levels of the $D\,^2\Sigma^-$ and $3\,^2\Sigma^-$ states, but none were observed.

The OH lines in the REMPI spectra displayed in Figs. 3–5 exhibit asymmetrically broadened line shapes with shading to higher energy. The experimentally observed line shape is attributed to the ac Stark effect, which results from the high power density of the laser. This type of line shape is common in nonlinear spectroscopy and is generally referred to as the optical or dynamical Stark effect, light shifts, or the Autler-Townes effect.[46,47] The breadth of the OH lines is on the order of 1.5 cm^{-1} half-width at half maximum (HWHM) as compared to an effective two-photon laser resolution of 0.5 cm^{-1}. The observed breadth is far greater than anticipated from lifetime broadening. The Rydberg states are computed to have 40–400 ps lifetimes with corresponding homogeneous linewidths of less than 0.1 cm^{-1}.[21]

The spectral data was analyzed to obtain band origins and rotational constants for the new transitions to the $D\,^2\Sigma^-(v'=3)$ and $3\,^2\Sigma^-(v'=1)$ as well as all lower vibrational levels in these Rydberg states. An energy-level diagram illustrating the upper and lower states involved in the two-photon $^2\Sigma^-$-$X\,^2\Pi_{3/2}$ transitions is shown in Fig. 6. The Λ-doublet spacing in the $X\,^2\Pi_{3/2}$ is exaggerated to show that the $Q_1(1)$ and $S_1(1)$ lines originate from the upper Λ-doublet component (f symmetry) and the $R_1(1)$ line originates from the lower Λ-doublet component (e symmetry) of the lowest

TABLE I. Spectroscopic constants including band origins (T_v), vibrational energies [$G(v)$], rotational constants (B_v), and spin-rotation constants (γ_v) derived for vibronic levels of the $D\,^2\Sigma^-$ and $3\,^2\Sigma^-$ Rydberg states of OH from this and previous experimental studies.

	T_v[a] (cm^{-1})	$G(v)$ (cm^{-1})	B_v[b,c] (cm^{-1})	γ_v[d] (cm^{-1})	Reference
			$D\,^2\Sigma^-$		
$v'=0$	81 789.4(5)	0	15.0(2)	−0.5	This work
	81 799(1)	0			16
	81 815.8	0	15.22	−0.5	17
	81 795.8(5)	0	15.24(2)	−0.37(7)	18
	81 797.95	0	15.218	−0.293	20
$v'=1$	84 364.1(5)	2566(2)	14.8(1)	−0.3	This work
	84 365.1	2549.3	14.79	−0.3	17
	84 349(15)	2550	14.83(3)	−0.37(13)	18
$v'=2$	86 865.3(5)	5067(2)	14.2(2)	−0.4	This work
	86 866.1	5050.3	14.30	−0.4	17
$v'=3$	89 285.1(5)	7487(2)	13.6(2)	−0.4	This work
			$3\,^2\Sigma^-$		
$v'=0$	87642.4(5)	0	14.9(1)	−0.2	This work
	87643.7	0	14.90	−0.2	17
$v'=1$	90282.6(5)	2640(2)	14.1(2)	−0.2	This work

[a] T_v values are for transitions from $X\,^2\Pi_{3/2}$ ($v''=0$) evaluated at the peak of the asymmetric line profile. Uncertainty in T_v is estimated from the effective two-photon linewidth arising from the laser bandwidth.
[b] de Beer *et al.*,[17] Collard *et al.*,[18] and Douglas[20] include D_v in their analysis, which is not taken into account in the present work with low J transitions only.
[c] B_v values from this work include data from all transitions that access a given v' level and its uncertainty is derived from a statistical analysis of the multiple measurements.
[d] In this work, γ_v is fixed at the de Beer *et al.*[17] value or their value for the next lower v'.

rotational level ($J=3/2$). All three lines are the main branch transitions ($\Delta J=\Delta N$) that access F_1 levels in the $^2\Sigma^-$ Rydberg state. The following standard expression is used to define the F_1 energy levels in a $^2\Sigma^-$ state in terms of the upper state constants,

$$F_1(N') = T_v + B_v N'(N'+1) + \tfrac{1}{2}\gamma N',$$

where $J'=N'+\frac{1}{2}$. The spin splitting constant γ was shown to be negative (ranging from -0.2 to -0.5 cm^{-1}) for lower vibrational levels in these Rydberg states, effectively shifting the rotational levels to lower energy by $\frac{1}{2}\gamma N'$. The spacings between the N' rotational levels accessed by the $Q_1(1)$, $R_1(1)$, and $S_1(1)$ lines are $4B_v+\gamma/2$ and $6B_v+\gamma/2$. The γ constant could not be determined directly from these two spacings in our measurements because of the experimental linewidth. Instead, we assume that the spin splitting constant for each of the newly observed levels is approximately equal to the previously determined value for the next lower vibrational level,[17] as listed in Table I. Fortunately, at low J, the $\gamma/2$ term is sufficiently small that it does not significantly affect the resultant B_v values.

Combination differences associated with the $Q_1(1)$, $R_1(1)$, and $S_1(1)$ lines for each vibronic transition were then used to determine the rotational constants B_v, with the small ground-state Λ-doublet splitting (0.055 cm^{-1} for $J=3/2$) (Ref. 1) taken into account. Multiple measurements of B_v derived from several spectral transitions that access the same v' were averaged to determine the B_v values and the associated uncertainties given in Table I. The vibronic origin T_v [equivalent to the unobserved $P_1(1)$ transition frequency] was then computed from the $Q_1(1)$ line position, upper state B_v value, and ground state Λ-doublet spacing. Table I lists the T_v, $G(v)$, B_v, and γ_v values for each vibrational level in the $D\,^2\Sigma^-$ and $3\,^2\Sigma^-$ Rydberg states accessed in the present experiments as well as previously reported values.

As pointed out recently by McRaven *et al.*,[16] there has been a discrepancy in the literature concerning the T_0 value for the $D\,^2\Sigma^-$ state of OH. McRaven *et al.* report $T_0=81\,799(1)$ cm^{-1} as compared to the values determined by de Beer *et al.*,[17] Collard *et al.*,[18] and Douglas[20] of 81 815.8, 81 795.8(5), and 81 797.95 cm^{-1}, respectively. The value obtained in the present study, $T_0=81\,798.4(5)$ cm^{-1}, is in excellent accord with the latest result of McRaven *et al.*[16] These values are also in reasonably good agreement with the studies of Collard *et al.* and Douglas, but not with the study of de Beer *et al.* Other results reported by de Beer *et al.*,[17] especially those dependent on the relative frequency of their laser, are in much better agreement with the present results (see Table I).

The enhanced sensitivity for (2+1) REMPI spectra of OH with hexapole focusing has also allowed us to observe numerous transitions to the $D\,^2\Sigma^-$ and $3\,^2\Sigma^-$ Rydberg states originating from the excited vibrational levels of the ground $X\,^2\Pi_{3/2}$ state, specifically $v''=1-3$, which are listed in Table II. The OH radicals are created and vibrationally excited in the pulsed discharge source, and then cooled—at least rotationally—in the ensuing supersonic expansion. The population in the excited vibrational states is not substantially relaxed in the expansion, presumably due to the large vibrational energy spacings. In a previous photodissociation

TABLE II. Matrix of the experimental vibronic origins (T_v,cm^{-1}) [the uncertainty of T_v values for transitions from $X\,^2\Pi_{3/2}$ ($v''=1-3$) is estimated as the breadth (HWHM) of the asymmetric line profiles] and calculated two-photon cross sections ($\hat{\sigma}^{(2)}$,10^{-38} cm^4) [calculated two-photon cross sections (integrated over line profile) from the accompanying theory paper (Ref. 21)] for OH transitions from $X\,^2\Pi(v'')$ to $D\,^2\Sigma^-(v')$ and $3\,^2\Sigma^-(v')$ Rydberg states.

	$X\,^2\Pi$	$v''=0$	$v''=1$	$v''=2$	$v''=3$
			$D\,^2\Sigma^-$		
$v'=0$	T_v	81 798.4	78 231.4	[a]	[a]
	$\hat{\sigma}^{(2)}$	2.57	3.88E−1	1.39E−2	5.84E−3
$v'=1$	T_v	84 364.1	80 793.3	77 392.5	[b]
	$\hat{\sigma}^{(2)}$	1.52	4.90E−1	4.41E−1	6.42E−2
$v'=2$	T_v	86 865.3	83 292.4	[b]	[c]
	$\hat{\sigma}^{(2)}$	5.86E−1	1.04	5.47E−2	4.08E−1
$v'=3$	T_v	89 285.1	85 714.2	82 309.6	[b]
	$\hat{\sigma}^{(2)}$	1.72E−1	8.07E−1	4.96E−1	7.24E−5
$v'=4$	T_v	[b]	[b]	[b]	[b]
	$\hat{\sigma}^{(2)}$	4.71E−2	4.46E−1	6.85E−1	2.34E−1
			$3\,^2\Sigma^-$		
$v'=0$	T_v	87 642.4	84 074.3	80 671.2	77 431.3[d]
	$\hat{\sigma}^{(2)}$	1.61	2.31	1.12	1.89E−1
$v'=1$	T_v	90 282.6	86 713.5	83 306.0	80 074.7
	$\hat{\sigma}^{(2)}$	2.69E−1	4.16E−1	2.82	2.38
$v'=2$	T_v	[b]	[b]	[b]	[b]
	$\hat{\sigma}^{(2)}$	1.03E−2	3.70E−1	1.55E−2	2.55
$v'=3$	T_v	[a]	[b]	[b]	[b]
	$\hat{\sigma}^{(2)}$	6.83E−4	5.59E−2	3.59E−1	5.99E−2

[a]Transitions were not scanned in most cases because they required a frequency-doubled Nd:YAG pumped dye laser.
[b]Searches were made for these transitions but they were not observed.
[c]A very weak transition was observed near 76 670 cm^{-1}.
[d]A water line overlaps the $S_1(1)$ line of this very weak OH transition making its identification very tentative.

study of OD at 226 and 243 nm,[24] we estimated a vibrational temperature of approximately 1700 K to account for the relative population of OD $X\,^2\Pi_{3/2}(v'')$ that was promoted to the repulsive $1\,^2\Sigma^-$ state. At this vibrational temperature, the $v''=1-3$ states of OH would contain only 5%, 0.3%, and, 0.002% of the total population. Nevertheless, (2+1) REMPI transitions are observed from each of these states ($v''=1-3$) to the $v''=0$ and 1 levels of the $3\,^2\Sigma^-$ Rydberg state. Fewer transitions are observed in the $D\,^2\Sigma^-$ Rydberg state, most of which originate from the $v''=0$, 1 levels of the ground $X\,^2\Pi$ state. Only the $D\,^2\Sigma^-(v'=1)$-$X\,^2\Pi(v''=2)$ and $D\,^2\Sigma^-(v'=3)$-$X\,^2\Pi(v''=2)$ transitions are detected from $v''=2$, and only a very weak transition is observed originating from $v''=3$.

A vibronic band was assigned only if both the $Q_1(1)$ and $S_1(1)$ lines could be identified under hexapole focusing conditions. The vibronic origins derived from the observed transitions are given in Table II. Assignments of the newly observed transitions to the $^2\Sigma^-$ Rydberg states were checked for consistency with the well-known vibrational spacings $G(v'')$ in the ground $X\,^2\Pi$ state.[1] In addition, vibrational spacings $G(v')$ in the $D\,^2\Sigma^-$ and $3\,^2\Sigma^-$ states associated with the transitions from excited vibrational levels of the ground $X\,^2\Pi$ state were found to be in accord with those given in Table I.

IV. DISCUSSION

The current experimental study yields simplified (2+1) REMPI spectra of the OH radical through hexapole state selection and focusing of a supersonic beam. The radicals are generated in a pulsed discharge source that is shown to produce rotationally cold, albeit vibrationally hot OH radicals.[24] Transitions are observed from the hexapole-selected OH $X\,^2\Pi_{3/2}(J=3/2,f)$ state in several vibrational levels, $v''=0-3$, to various rovibrational levels in the nested $D\,^2\Sigma^-$ and $3\,^2\Sigma^-$ Rydberg states. Transitions are observed to the $D\,^2\Sigma^-(v'=0-3)$ and $3\,^2\Sigma^-(v'=0,1)$ vibronic levels, which extends previous studies to higher vibrational levels in the Rydberg states. Transitions to yet higher vibrational levels are not observed.

A spectroscopic analysis has been performed to ascertain the vibronic origin T_v and upper-state rotational constant B_v associated with each vibronic band (Table I). The vibronic origins are used to determine the vibrational energies $G(v)$ of the observed levels in the $D\,^2\Sigma^-$ and $3\,^2\Sigma^-$ states, which are listed in Table I. A weighted least-square fit of the $G(v)$ values is then carried out to estimate the harmonic frequency $\omega_e=2642.2(9)$ cm^{-1} and anharmonicity constant $\omega_e x_e=36.8(3)$ cm^{-1} for the $D\,^2\Sigma^-$ state. Since only one vibrational spacing is available for the $3\,^2\Sigma^-$ state, analogous vibrational parameters cannot be determined. Similarly, a weighted least-squares fit of B_v values is performed to determine the rotational constants $B_e=15.5(2)$ cm^{-1} and $\alpha_e=0.51(9)$ cm^{-1} at the equilibrium position of the $D\,^2\Sigma^-$ state, along with the corresponding internuclear separation distance $R_e=1.072(5)$ Å. The B_e and α_e constants for the $3\,^2\Sigma^-$

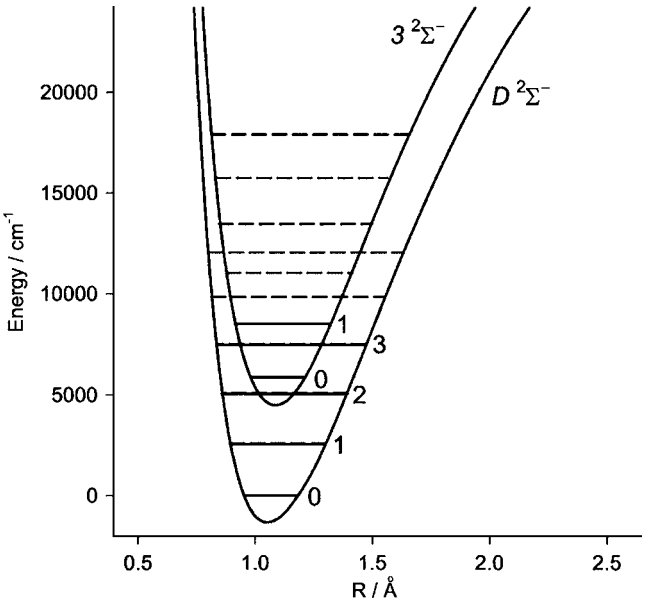

FIG. 7. Experimentally observed (solid) and computed (dashed) vibrational levels supported by the $D\ ^2\Sigma^-$ and $3\ ^2\Sigma^-$ Rydberg states of OH. The *ab initio* potentials and associated vibrational levels (dashed) have been shifted slightly to be in better accord with experiment (see Ref. 21).

state are determined to be 15.3(1) and 0.8(2) cm^{-1}, along with R_e=1.078(3) Å, based on the two available B_v values.

Comparison of the spectroscopic parameters derived in this work with those from previous experimental studies is possible only for transitions originating from the $X\ ^2\Pi_{3/2}(v''=0)$ state, as shown in Table I. Transitions originating from excited vibrational levels of the $X\ ^2\Pi_{3/2}$ state (Table II) have not been reported previously. The vibronic origin of the $D\ ^2\Sigma^-(v'=0)$-$X\ ^2\Pi(v''=0)$ transition in the present work is consistent with the value obtained in a recent (1+1) REMPI study,[16] resolving a discrepancy in an earlier report.[17] Excluding this earlier report of T_0,[17] there is very good agreement between the vibronic origins reported here and those deduced in previous studies of transitions to the $D\ ^2\Sigma^-(v'=0-2)$ and $3\ ^2\Sigma^-(v'=0)$ states.[16–18,20] Similarly, there is good accord between the rotational constants presented here and those obtained in previous studies.[17,18,20] Additionally, the equilibrium rotational constant and bond length derived here for the $D\ ^2\Sigma^-$ state agree with a previous determination of these parameters.[18] However, the vibrational constants estimated in that same study[18] using isotopic data do not agree with current results, most likely because of the limited $G(v)$ data available at that time.

The spectroscopic observables are compared with the corresponding properties derived from *ab initio* potentials of the $D\ ^2\Sigma^-$ and $3\ ^2\Sigma^-$ Rydberg states in the accompanying paper.[21] The *ab initio* potentials are then adjusted to match the experimental data reported here for the vibrational energies and rotational constants of the Rydberg states. The calculated parameters for the adjusted potentials match the experimental $G(v)$ values to within 0.2% and B_v values to within 2.5%, which is nearly quantitative agreement. This is illustrated in Fig. 7, which shows the experimentally observed and computed vibrational levels supported by the Rydberg states. The equilibrium bond lengths for the $D\ ^2\Sigma^-$ and $3\ ^2\Sigma^-$ states deduced from the adjusted potentials are 1.06 and 1.09 Å, respectively, which are in reasonably good agreement with the experimentally determined values of 1.072(5) and 1.078(3) Å.

The two-photon absorption cross sections $\hat{\sigma}^{(2)}$ for $D\ ^2\Sigma^-$-$X\ ^2\Pi$ and $3\ ^2\Sigma^-$-$X\ ^2\Pi$ transitions were also calculated from first principles in the companion paper.[21] The computed cross sections, integrated over the line profile, are listed in Table II in (v',v'') matrix format for comparison with the pattern of experimentally observed vibronic transitions. The largest two-photon cross section is predicted for the $D\ ^2\Sigma^-(v'=0)$-$X\ ^2\Pi(v''=0)$ transition with $\hat{\sigma}^{(2)}=2.57\times10^{-38}$ cm^4.[21] The cross section for this transition can be compared to those for other atomic and molecular species. For example, the two-photon cross section for the $3p\ ^3P_{2,1,0}-2p\ ^3P_2$ transition of atomic oxygen is 1000 times stronger at 2.66×10^{-35} cm^4.[48] In addition, the two-photon cross section for the $E/F\ ^1\Sigma_g(v'=6)$-$X\ ^1\Sigma_g(v''=0)$ transition of molecular hydrogen has been determined experimentally[49] (2.0×10^{-36} cm^4) and theoretically[50] (2.8×10^{-36} cm^4) to be about 100 times stronger than that predicted for OH. On the other hand, the experimentally determined two-photon cross section for the $R_{22}+S_{12}(J''=9.5)$ lines of the $A\ ^2\Sigma^+(v'=0)$ -$X\ ^2\Pi(v''=0)$ transition of NO is 1.5×10^{-38} cm^4,[51] which is two times weaker than that predicted for OH. Thus, the magnitude of the two-photon cross section suggests that OH should be a good candidate for (2+1) REMPI detection. However, it still requires an efficient ionization step, specifically, a reasonably long-lived intermediate state and a large ionization cross section.

The radiative lifetimes of the $D\ ^2\Sigma^-$ and $3\ ^2\Sigma^-$ Rydberg states are computed to be reasonably long in the early work of van Dishoeck and Delgarno[22] (~10 ns) as well as in the companion theoretical study (1.5–3.5 ns).[21] These lifetimes are sufficiently long that radiative decay from the Rydberg states should not cause a substantial loss of population prior to ionization with a 4–6 ns or shorter laser pulse. On the other hand, electronic predissociation of the Rydberg states through spin-orbit coupling with the repulsive $B\ ^2\Sigma^+$, $2\ ^2\Pi$, and $1\ ^4\Pi$ potentials could provide a much more efficient loss mechanism. Indeed, this has been suggested for some time,[17,22] but without experimental or theoretical verification. The calculations presented in the accompanying paper indicate overall lifetimes for the $D\ ^2\Sigma^-(v')$ and $3\ ^2\Sigma^-(v')$ states of 40–400 ps,[21] which is at least ten times faster than radiative decay alone. The rapid decay is attributed primarily to coupling with the $2\ ^2\Pi$ and $1\ ^4\Pi$ potentials (see Ref. 21). The rapid electronic predissociation of the Rydberg states is expected to compete effectively with ionization when using nanosecond lasers, resulting in a lower ionization yields and less sensitive detection of OH via (2+1) REMPI. Shorter pulsed lasers of picosecond duration should be much more effective in photoionization detection of OH.

A closer examination of Table II allows for comparison of calculated two-photon cross sections with experimental observations for transitions originating from specific $X\ ^2\Pi$ (v'') levels. If one considers transitions to $D\ ^2\Sigma^-$ $(v'=0-3)$ and $3\ ^2\Sigma^-$ $(v'=0,1)$ states only, there is an extremely good correlation between the magnitude of the two-photon cross

section and the observation of the corresponding transition by (2+1) REMPI. Transitions that are not observed experimentally, e.g., $D\,^2\Sigma^-$ $(v'=2)-X\,^2\Pi$ $(v''=2)$, are predicted to have significantly smaller cross sections than those for observed transitions from the same $X\,^2\Pi$ (v'') level. By contrast, the magnitudes of the two-photon cross sections for transitions to higher vibrational levels in the Rydberg states are not consistent with the lack of observable transitions to these levels. In fact, several transitions are predicted to have larger cross sections, e.g., $D\,^2\Sigma^-$ $(v'=4)-X\,^2\Pi$ $(v''=1$ or $2)$, than those for observed transitions from the same $X\,^2\Pi$ (v'') level. This indicates that predissociation of $D\,^2\Sigma^-$ $(v'\geqslant 4)$ and $3\,^2\Sigma^-$ $(v'\geqslant 2)$ is much faster than that found for lower vibrational levels in the Rydberg states. The companion theory paper,[21] however, does not indicate an abrupt decrease in lifetimes for higher vibrational levels. This suggests that additional perturbations from one or more higher-lying states may be responsible for the lack of observable transitions to the $D\,^2\Sigma^-$ $(v'\geqslant 4)$ and $3\,^2\Sigma^-$ $(v'\geqslant 2)$ levels. The perturbing state(s) would need to cross the Rydberg states about 10 000 cm^{-1} above the vibrationless level of the $D\,^2\Sigma^-$ state (see Fig. 7) to account for the lack of observable transitions to these higher vibrational levels.

Ionization cross sections for the OH $D\,^2\Sigma^-$ and $3\,^2\Sigma^-$ Rydberg states in the 4.8–5.6 eV photon energy range have been estimated theoretically by Stephens and McKoy.[52] At around 5.5 eV, the $D\,^2\Sigma^-$ $(v'=0)$ ionization cross section is estimated to be $\sigma_{\text{ioniz}}\sim 5\times 10^{-19}$ cm^2. This same value has been measured by Bamford *et al.*[48] for the photoionization of O (^3P) atoms at 226 nm (5.5 eV). There have been no experimental measurements of σ_{ioniz} for the OH $D\,^2\Sigma^-$ or $3\,^2\Sigma^-$ states, although we suspect the value may be lower than the theoretical estimate. McRaven *et al.*[16] found it necessary to tightly focus their 320 nm (3.9 eV) ionization laser to efficiently ionize the predissociative $D\,^2\Sigma^-$ $(v'=0)$ state, which would suggest a smaller σ_{ioniz} than that for O (^3P) atoms.

Finally, it should be noted that the observation of many transitions from OH $X\,^2\Pi$ $(v''=1-3)$ suggests a much higher vibrational temperature than the 1700 K used to simulate the earlier photodissociation results.[24] The discharge conditions were adjusted over the course of the measurements to optimize signals for these hot band transitions, and thus we do not attempt to estimate a vibrational distribution based on the observed REMPI transitions. No attempt was made to search for REMPI transitions originating from OH $X\,^2\Pi$ $(v''\geqslant 4)$, which were found to contribute to the photodissociation results. This could be examined in future work. It should be emphasized that the rotational distribution from the discharge source used in REMPI and photodissociation studies was quite cold (see Fig. 3).

V. CONCLUSIONS

Two-photon transitions to the $D\,^2\Sigma^-$ and $3\,^2\Sigma^-$ Rydberg states of the OH radical have been characterized using (2+1) REMPI spectroscopy. The OH radicals are produced in a pulsed discharge source that yields rotationally cold, yet vibrationally hot radicals, which are then state selected and focused using a hexapole field. Simplified spectra consisting of predominately $Q_1(1)$ and $S_1(1)$ lines are observed originating from the selected $|M_J|=3/2$ component of the upper Λ-doublet level of the lowest rotational state $(J=3/2)$ for both ground $(v''=0)$ and excited $(v''=1-3)$ vibrational levels of the OH $X\,^2\Pi_{3/2}$ state. Transitions are observed to the $D\,^2\Sigma^-$ $(v'=0-3)$ and $3\,^2\Sigma^-$ $(v'=0,1)$ vibronic levels, thereby extending previous studies to higher vibrational levels in each of the Rydberg states. Yet higher vibronic levels are not observed, presumably due to an additional perturbing state that has not been identified. Spectroscopic parameters derived in this work are generally in accord with prior studies of the lower vibronic levels.

The spectroscopic observables are used to calibrate new *ab initio* potentials for the Rydberg states, as described in the accompanying paper, which are then used for detailed calculations of the properties of the $D\,^2\Sigma^-$ and $3\,^2\Sigma^-$ states.[21] The experimentally observed transitions from a given $X\,^2\Pi$ (v'') level to a specific vibronic level in the Rydberg states show a good correlation with the calculated two-photon absorption cross sections.[21] The short predissociation lifetimes of 40–400 ps computed for the $D\,^2\Sigma^-$ (v') and $3\,^2\Sigma^-$ (v') Rydberg states,[21] however, indicate an efficient loss mechanism that could compete effectively with ionization when using nanosecond lasers. This suggests that picosecond lasers may be more effective in photoionization detection of the OH radical.

ACKNOWLEDGMENTS

Two of the authors (D.H.P) and (M.I.L.) thank the Dutch National Science Foundation (NWO) for a Visiting Professor Fellowship B70-316. The experimental work in The Netherlands is part of the research program of the FOM-NWO organization. Two of the authors (M.E.G.) and (M.I.L.) gratefully acknowledge the support from the Air Force Office of Scientific Research under Contract No. FA9550-04-1-0068.

[1] J. A. Coxon, Can. J. Phys. **58**, 933 (1980).
[2] D. R. Crosley, Adv. Ser. Phys. Chem. **3**, 256 (1995).
[3] G. H. Dieke and H. M. Crosswhite, J. Quant. Spectrosc. Radiat. Transf. **2**, 97 (1962).
[4] G. Ondrey, N. van Veen, and R. Bersohn, J. Chem. Phys. **78**, 3732 (1983).
[5] D. E. Heard and M. J. Pilling, Chem. Rev. (Washington, D.C.) **103**, 5163 (2003).
[6] R. A. Copeland, J. B. Jeffries, and D. R. Crosley, Chem. Phys. Lett. **138**, 425 (1987).
[7] J. A. Coxon, A. D. Sappey, and R. A. Copeland, J. Mol. Spectrosc. **145**, 41 (1991).
[8] A. D. Sappey, D. R. Crosley, and R. A. Copeland, J. Chem. Phys. **90**, 3484 (1989).
[9] A. D. Sappey and R. A. Copeland, J. Chem. Phys. **93**, 5741 (1990).
[10] A. D. Sappey and R. A. Copeland, J. Mol. Spectrosc. **143**, 160 (1990).
[11] E. S. Hwang, J. B. Lipson, R. W. Field, and J. A. Dodd, J. Phys. Chem. A **105**, 6030 (2001).
[12] P. Casavecchia, N. Balucani, and G. G. Volpi, Adv. Ser. Phys. Chem. **6**, 365 (1995).
[13] D. M. Sonnenfroh, R. G. Macdonald, and K. Liu, J. Chem. Phys. **94**, 6508 (1991).
[14] S. Y. T. van de Meerakker, P. H. M. Smeets, N. Vanhaecke, R. T. Jongma, and G. Meijer, Phys. Rev. Lett. **94**, 023004 (2005).
[15] J. R. Bochinski, E. R. Hudson, H. J. Lewandowski, G. Meijer, and J. Ye, Phys. Rev. Lett. **91**, 243001 (2003).
[16] C. McRaven, J. Alnis, B. Furneaux, and N. Shafer-Ray, J. Phys. Chem. A **107**, 7138 (2003).

[17] E. de Beer, M. P. Koopmans, C. A. de Lange, Y. Wang, and W. A. Chupka, J. Chem. Phys. **94**, 7634 (1991).
[18] M. Collard, P. Kerwin, and A. Hodgson, Chem. Phys. Lett. **179**, 422 (1991).
[19] R. Forster, H. Hippler, K. Hoyermann, G. Rohde, and L. B. Harding, Chem. Phys. Lett. **183**, 465 (1991).
[20] A. E. Douglas, Can. J. Phys. **52**, 318 (1974).
[21] M. P. J. van der Loo and G. C. Groenenboom, J. Chem. Phys. **123**, 074310 (2005), following paper.
[22] E. F. van Dishoeck and A. Dalgarno, J. Chem. Phys. **79**, 873 (1983).
[23] E. F. van Dishoeck, S. R. Langhoff, and A. Dalgarno, J. Chem. Phys. **78**, 4552 (1983).
[24] D. C. Radenovic, A. J. A. van Roij, D. A. Chestakov *et al.*, J. Chem. Phys. **119**, 9341 (2003).
[25] H.-J. Werner and P. J. Knowles, J. Chem. Phys. **89**, 5803 (1988).
[26] P. J. Knowles and H.-J. Werner, Chem. Phys. Lett. **145**, 514 (1988).
[27] H.-J. Werner, P. J. Knowles, M. Schütz *et al.*, MOLPRO package of *ab initio* programs.
[28] M. C. van Beek and J. J. ter Meulen, Chem. Phys. Lett. **337**, 237 (2001).
[29] The average pressure in the primary chamber is 2×10^{-5} mbar when the pulsed discharge is operating. The source chamber is separated from the detection chamber by a skimmer (2 mm diameter, 12.5 mm downstream of the orifice). The detection chamber is held at $\leqslant10^{-6}$ mbar using a turbo molecular pump.
[30] K. Schreel and J. J. ter Meulen, J. Phys. Chem. A **101**, 7639 (1997).
[31] T. D. Hain, M. A. Weibel, K. M. Backstrand, and T. J. Curtiss, J. Phys. Chem. A **101**, 7674 (1997).
[32] T. D. Hain and T. J. Curtiss, J. Phys. Chem. A **102**, 9696 (1998).
[33] K. Ikejiri, H. Ohoyama, Y. Nagamachi, T. Teramoto, and T. Kasai, Chem. Phys. Lett. **379**, 255 (2003).
[34] M. C. van Beek, J. J. ter Meulen, and M. H. Alexander, J. Chem. Phys. **113**, 628 (2000).
[35] R. J. Yokelson, R. J. Lipert, and W. A. Chupka, J. Chem. Phys. **97**, 6153 (1992).
[36] K. P. Huber and G. Herzberg, *Molecular Spectra and Molecular Structure IV. Constants of Diatomic Molecules* (Van Nostrand Reinhold, New York, 1979).
[37] W. C. Martin, J. R. Fuhr, D. E. Kelleher *et al.*, http://physics.nist.gov/asd, version 2.0, National Institute of Standards and Technology, Gaithersburg, MD, 2002.
[38] X. Zhu, A. H. Nur, and P. Misra, J. Quant. Spectrosc. Radiat. Transf. **52**, 167 (1994).
[39] D. H. Parker, Acc. Chem. Res. **33**, 563 (2000).
[40] The repeller plate had a 3-mm-diameter opening, while the extractor and ground plates had 20-mm center holes. Typical voltages applied to the repeller and extractor plates are 2.0 and 1.5 kV, respectively.
[41] E. de Beer, Ph.D. thesis, University of Amsterdam, 1993.
[42] K. Schreel, J. Schleipen, A. Eppink, and J. J. ter Meulen, J. Chem. Phys. **99**, 8713 (1993).
[43] M. van Beek, Ph.D. thesis, Katholieke Universiteit Nijmegen, 2001.
[44] D. T. Anderson and M. I. Lester, J. Phys. Chem. A **107**, 2606 (2003).
[45] H. Dickinson, S. R. Mackenzie, and T. P. Softley, Phys. Chem. Chem. Phys. **2**, 4669 (2000).
[46] B. Girard, G. O. Sitz, R. N. Zare, N. Billy, and J. Vigue, J. Chem. Phys. **97**, 26 (1992).
[47] B. Girard, N. Billy, J. Vigue, and J. C. Lehmann, Chem. Phys. Lett. **102**, 168 (1983).
[48] D. J. Bamford, L. E. Jusinski, and W. K. Bischel, Phys. Rev. A **34**, 185 (1986).
[49] J. D. Buck, D. C. Robie, A. P. Hickman, D. J. Bamford, and W. K. Bischel, Phys. Rev. A **39**, 3932 (1989).
[50] W. M. Huo and R. L. Jaffe, Chem. Phys. Lett. **101**, 463 (1983).
[51] J. Burris and T. J. McIlrath, J. Opt. Soc. Am. B **2**, 1307 (1985).
[52] J. A. Stephens and V. McKoy, J. Chem. Phys. **93**, 7863 (1990).